Journal of Solid State Chemistry **146,** 96–102 (1999)
Article ID jssc.1999.8313, available online at http://www.idealibrary.com on IDEAL®

Synthesis and Properties of the Structurally One-Dimensional Cobalt Oxide $Ba_{1-x}Sr_xCoO_3$ ($0 \leq x \leq 0.5$)

K. Yamaura,*,[1] H. W. Zandbergen,† K. Abe,* and R. J. Cava*

*Department of Chemistry and Princeton Materials Institute, Princeton University, Princeton, New Jersey 08540; and †National Institute for HREM, Laboratory for Materials Science, Delft University of Technology, 2628 AL Delft, The Netherlands

Received January 6, 1999; accepted April 7, 1999

The hexagonal perovskite solid solution $Ba_{1-x}Sr_xCoO_3$ ($0 \leq x \leq 0.5$) was synthesized by treatment of cubic perovskite precursors at 500°C in high-pressure oxygen. The structure consists of parallel chains of face-sharing CoO_6 octahedra and alkaline-earth ion separators. All materials were found to be semiconducting. Seebeck coefficient measurements indicate that transport is by both electrons and holes. The slopes of the magnetic susceptibility vs temperature data suggest that Co is in the low-spin $S=1/2$ electronic configuration. The positive Curie–Weiss Θ_w's indicate a predominantly ferromagnetic spin interaction, and a complex magnetic state is seen at low temperature in the temperature- and field-dependent magnetic data.

Key Words: **$BaCoO_3$; hexagonal perovskite; chain structure; low-dimensional magnetism.**

INTRODUCTION

To construct models for correlated electron behavior in solids, many experimental and theoretical studies have concentrated on one-dimensional (1D) systems, as in such systems there is the realistic possibility that experimental results can be successfully analyzed through theoretical models. Novel phenomena which are the consequence of electron correlations have often been found in 1D compounds (1). $BaCoO_3$ is a structurally 1D compound because it has the hexagonal perovskite structure ($P6_3/mmc$; $a = 0.5645(3)$ nm and $c = 0.4752(3)$ nm (2)) formed by 1D chains of face-sharing CoO_6 octahedra and Ba separators. Two views of $BaCoO_3$, showing the structural anisotropy, are shown in Fig. 1. The structure type is generally known as the "2H type"; i.e., the stacking sequence unit along the c axis of the hexagonal phase has two BaO_3 layers before repeating. The distance between the Co within the chain, 0.238 nm, is much shorter than the interchain distance, 0.565 nm. The chains themselves are arranged in a triangular geometry which may at least partially frustrate long-range order if the magnetic interactions between chains are antiferromagnetic. There are no Co–O–Co links between chains (2). As in many of the transition metal oxides (e.g., the cuprates) presently actively under study, the presence of significant oxygen p character in electronic states near the Fermi energy may be expected to ameliorate the extreme one-dimensional character of the structure and can result in decreased electronic anisotropy.

Previous research on $BaCoO_3$ has indicated that it is semiconducting (3). The origin of the semiconducting behavior, however, is unclear. Several possibilities can be considered: (i) The low symmetry of the 2H-type structure may produce an energy gap at the Fermi level even at the partial band filling expected for low-spin Co^{4+} ($t_{2g}^5 e_g^0$). Although there are no spectroscopic measurements presently available on $BaCoO_3$, the charge-transfer-type electronic configuration, i.e., Co^{3+} ($t_{2g}^6 e_g^0$)$\underline{L}$($\underline{L}$: ligand hole), can be expected in this case, as was found in $NaCuO_2$ (4), $LiNiO_2$ (5, 6), and $SrFeO_3$ (7), for example. Even if such measurements are found to be consistent with an electronic configuration of Co^{3+} with one hole in oxygen p orbitals, $BaCoO_3$ would still be expected to be metallic. Indeed, the charge-transfer-type oxide $SrFeO_3$ is a metallic conductor (7). Moreover, the higher symmetry isoelectronic cubic perovskite $SrCoO_3$ has metallic conductivity down to 4.2 K (8). (ii) Strongly correlated electrons may produce an energy gap at the Fermi level. A Mott-Hubbard gap is for example produced at the Fermi level at ~ 70 K in $BaVS_3$, which also has the 2H-type structure (9), resulting in a metal–insulator transition. (iii) The Co chains could be dimerized along the c axis (so far unobserved), leading to the opening of a band gap. (iv) Due to the presence of some as-yet-undetected disorder in the structure, charge carriers could be scattered by random centers, particularly effective in low-dimensional systems, leading to Anderson localization.

Here, we report the synthesis and elementary transport and magnetic properties of the Sr-substituted 2H-type solid

[1]To whom correspondence should be addressed. Princeton Materials Institute, Bowen Hall, 70 Prospect Ave., Princeton, NJ 08540. Fax: +1-609-258-6878. E-mail: yama@princeton.edu.

0022-4596/99 $30.00

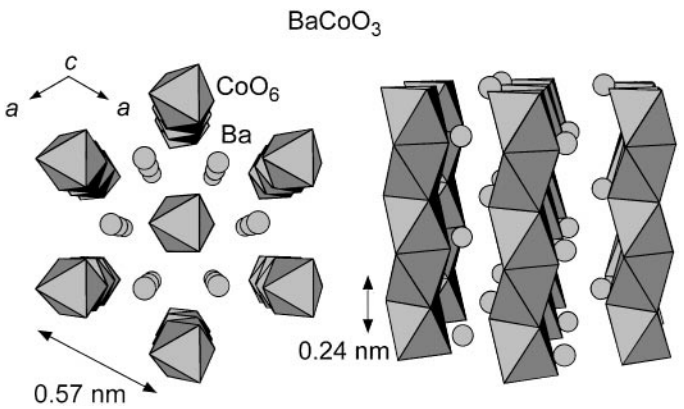

FIG. 1. Structural views of $BaCoO_3$. The CoO_6 octahedra are shown as polyhedra and the Ba as circles. The compound has a hexagonal unit cell ($P6_3/mmc$; $a = 0.5645(3)$ nm and $c = 0.4752(3)$ nm (2)).

solution $Ba_{1-x}Sr_xCoO_3$ for the range of composition $0 \leq x \leq 0.5$. This isoelectronic substitution changes the separation between the chains and, possibly, the O–Co–O superexchange bond angle and has a significant effect on the properties. Although the compound $BaCoO_3$ can be prepared under relatively conventional synthetic conditions, we have found that it is only possible to synthesize the Ba–Sr solid solution by a precursor route involving the formation of a perovskite. The synthesis conditions, characterization via X-ray diffraction (XRD), and the electrical and magnetic properties of the polycrystalline samples are reported here.

EXPERIMENTAL

Polycrystalline samples were synthesized as follows. Mixtures of $BaCO_3$ (99.95%), $SrCO_3$ (99.99%), and Co_3O_4 (99.9985%) with the ratios of $Ba:Sr:Co = 1-x:x:1$ ($x = 0$–0.5 with a 0.1 step) were heated at 800°C for 24 h in nitrogen. Subsequent to the initial heating, the samples were heated at 900°C for 24 h in nitrogen three times. After heating at 900°C, samples were pressed into pellets. The pellets were heated at 900°C in nitrogen for 24 h. Finally, the pellets were annealed at 500°C for 24 h in high-pressure oxygen (34.2 MPa, Morris Research high-pressure furnace). Alumina and gold crucibles were employed to hold the samples at elevated temperatures in the nitrogen and high-pressure oxygen treatments, respectively. Without this series of synthesis steps, the amount of Sr taken into solid solution in hexagonal $BaCoO_3$ was not significant.

Powder XRD with Cu$K\alpha$ radiation, and thermogravimetric analysis (TGA), were employed to characterize the samples after both the nitrogen and the high-pressure oxygen treatments. A small amount of fine silicon powder was mixed with each ground sample for XRD study as an internal standard. The oxygen content of the samples was determined by reduction to alkaline earth monoxides and Co metal in the TGA by heating in 10% hydrogen/90% nitrogen at a heating rate of 5 K/min to 800°C and holding for 8 or more h. One of the precursors was characterized by electron diffraction (ED) on a Phillips EM 200 electron microscope. The electrical resistivity of the final polycrystalline samples was measured between 77 and 320 K by a conventional four-probe ac technique with a gauge current of 11.1 μA at 132 Hz. Thermoelectric coefficients were measured in a commercial apparatus (MMR Technologies). A SQUID magnetometer (QUANTUM DESIGN MPMS5) was employed to characterize the magnetic properties of the samples between 5 and 400 K. The highest applied magnetic field was 55 kOe.

STRUCTURE AND STOICHIOMETRY

The precursor phase is not the subject of this study, but was characterized in a preliminary manner to allow understanding of the Sr–Ba solid solution limits in the hexagonal phase of interest. The powder XRD patterns for the nitrogen-treated precursors of composition $Ba_{1-x}Sr_xCoO_{2.5+y}$ are presented in Fig. 2. The XRD study revealed that for all samples with x greater than or equal to 0.2 a single-phase cubic material is formed. TGA analysis of these cubic phases indicated an oxygen content of 2.50(1) oxygen per formula unit, less than the ideal perovskite value of 3.0. Careful study of the composition $Ba_{0.8}Sr_{0.2}CoO_{2.50}$ by ED revealed that the unit cell was indeed a 3.9 Å cubic perovskite. There were no extra reflections, either sharp or diffuse, which would indicate that there is short-range or long-range ordering of

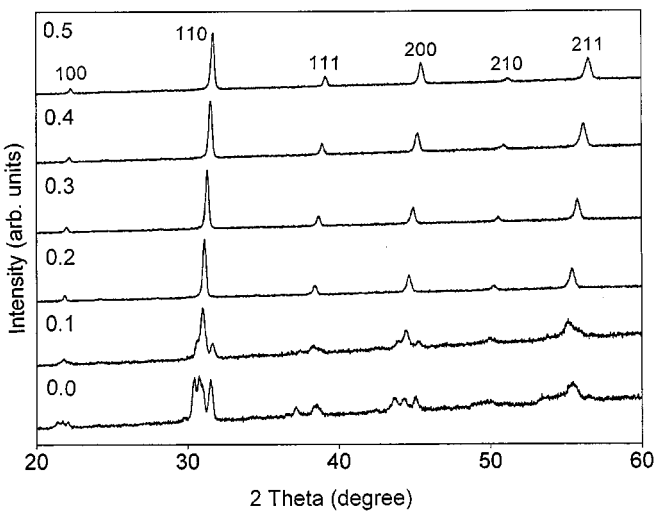

FIG. 2. Powder XRD patterns of the cubic and pseudocubic solid solutions $Ba_{1-x}Sr_xCoO_{2.5+y}$ ($0.0 \leq x \leq 0.5$). Numbers beside the left vertical axis, above each pattern, represent the value of x. The peaks for compositions greater than $x = 0.1$ can be indexed on a simple cubic unit cell. For $x = 0$ and 0.1, distortions from the simple cubic perovskite occur.

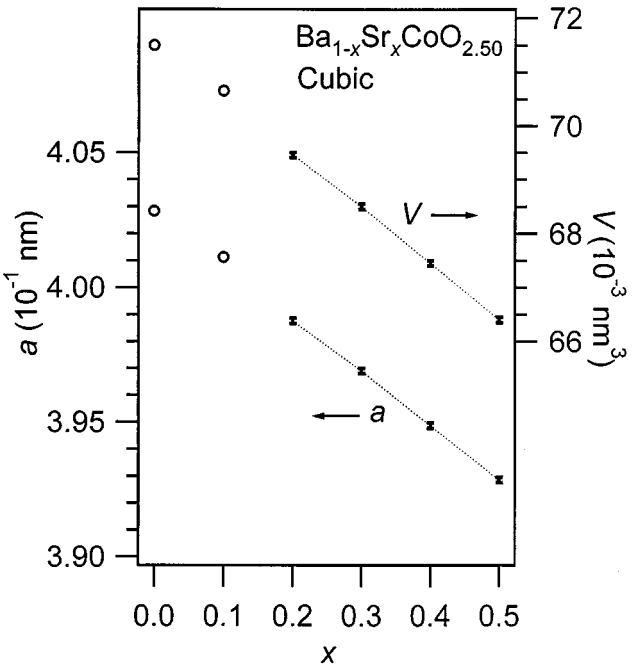

FIG. 3. Cubic lattice constant (a) and volume of the cubic unit cell (V) of $Ba_{1-x}Sr_xCoO_{2.50}$ ($0.2 \leq x \leq 0.5$). Open circles indicate average cell parameters at compositions of $x = 0$ and 0.1.

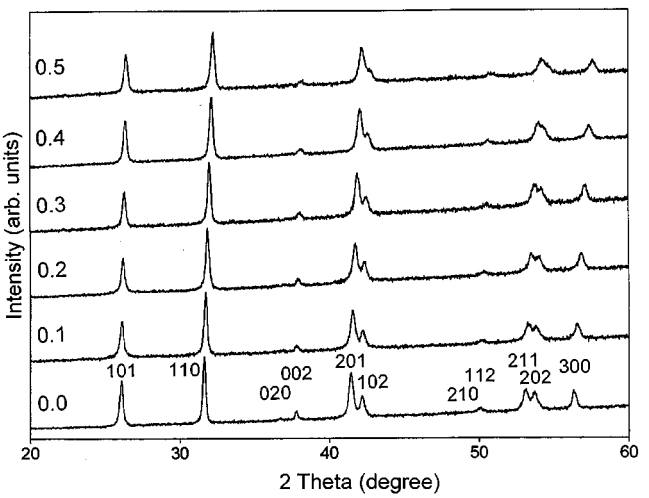

FIG. 4. Powder XRD patterns of the solid solutions $Ba_{1-x}Sr_xCoO_3$ ($0 \leq x \leq 0.5$). Numbers beside the left vertical axis, above each pattern, represent the value of x. The peaks at every composition can be indexed on a hexagonal unit cell as shown at the bottom of the pattern.

the oxygen vacancies under the conditions of synthesis. For $x = 0$ and 0.1 compositions, the XRD patterns reveal that the precursors are not simple cubic perovskites, but this was not further studied. Figure 3 shows the cubic cell parameter for the $Ba_{1-x}Sr_xCoO_{2.50}$ perovskite solid solution (for $x = 0$ and 0.1 average cell parameters are employed) as a function of Sr content. The formation of this cubic perovskite-like solid solution is essential for the later synthesis of the hexagonal phases. For Sr concentrations greater than $x = 0.5$, the single-phase cubic perovskite-like solid solution cannot be synthesized in nitrogen, the factor which we believe limits the extent of Sr content attainable in the 2H-type solid solution.

Figure 4 shows the powder XRD patterns for the $Ba_{1-x}Sr_xCoO_{2.5+y}$ perovskite solid solution materials after they have been heated at 500°C at high oxygen pressure. They are now single-phase 2H-type $Ba_{1-x}Sr_xCoO_3$ ($0 \leq x \leq 0.5$). The TGA study for these samples confirmed that they have stoichiometric oxygen contents within the precision of the TGA method, e.g., 2.99(1) oxygen per formula unit. The materials with the highest Sr contents, $Ba_{0.5}Sr_{0.5}CoO_z$ and $Ba_{0.6}Sr_{0.4}CoO_z$, appear to have a slight oxygen deficiency, $z = 2.97(1)$, under the conditions of synthesis. We have no information about how this very small oxygen deficiency is accommodated. It may occur either in randomly distributed vacant sites or in a small fraction of microdomains with a short-range ordering of vacancies. All the observed powder XRD peaks at $x = 0$ (i.e., $BaCoO_3$) were indexed on the basis of the hexagonal unit cell reported previously (2). The lattice constants at $x = 0$ determined in this study are identical to those previously reported. The observed peaks at other compositions were indexed by analogy. Lattice constants determined by least-squares fitting of the peak positions, and volumes of the unit cell derived from those constants, are plotted in Fig. 5. The increasing XRD peak width with increasing Sr content in the hexagonal phase tracks the peak widths in the cubic precursors, suggesting that it is due to small

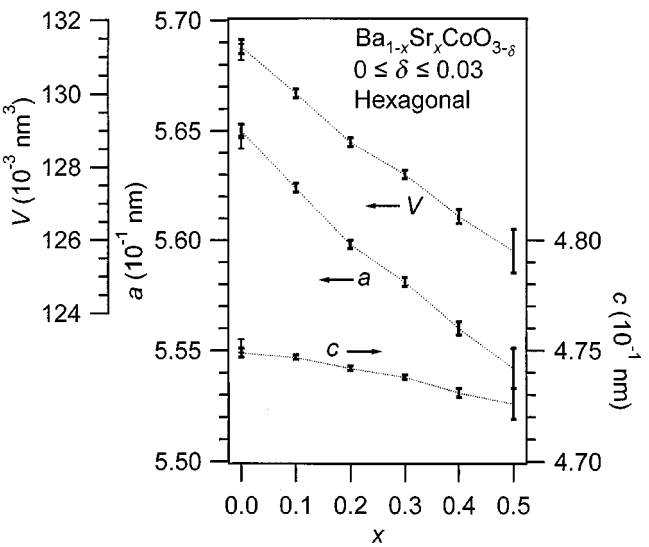

FIG. 5. Lattice constants (a and c) and hexagonal unit cell volume (V) of $Ba_{1-x}Sr_xCoO_3$ ($0 \leq x \leq 0.5$). Previously reported lattice constants for $BaCoO_3$ (2) are plotted with fine error bars.

inhomogeneities in Ba/Sr distribution. Alternatively, the excess peak widths may be due to the presence of defective structural layers, such as those found in $BaCoO_{3-\delta}$, stacked randomly along the c axis (10–12). Further study via electron microscopy would be required to identify the details of the defect structure of these compounds.

The lattice constants a and c decrease with increasing Sr concentration in the solid solution, as does the volume of the unit cell (V in Fig. 5), consistent with the smaller effective ionic radius for Sr than for Ba (13). The lattice constant a decreases by about 1.9% with the 50% Sr substitution for Ba, about four times larger than that of the c-lattice constant (0.48%). The Sr substitution therefore clearly decreases the separation between chains. The powder X-ray diffraction measurements do not provide information on possible changes in bond length or bond angle within the CoO_6 octahedra as a function of Sr content.

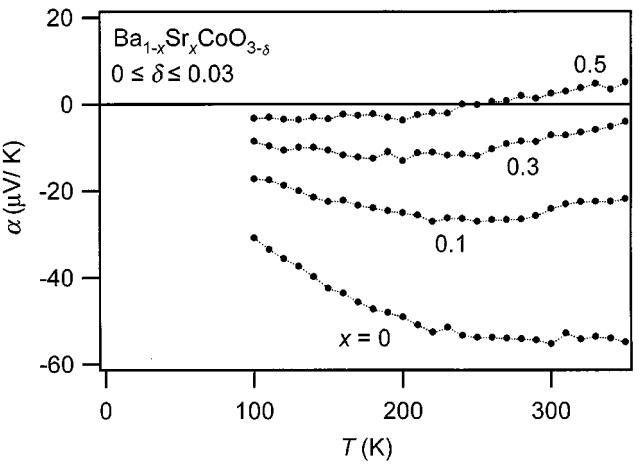

FIG. 7. The thermoelectric coefficients for $Ba_{1-x}Sr_xCoO_3$ ($0 \le x \le 0.5$) in the vicinity of ambient temperatures for selected compositions.

ELECTRICAL AND MAGNETIC PROPERTIES

The temperature dependence of the electrical resistivity of the samples is shown in Fig. 6. Semiconducting behavior is observed for all samples in the studied temperature range. The electrical resistivity of the 2H-type $Ba_{1-x}Sr_xCoO_3$ solid solution slowly decreases with increasing x: The resistivity is more than 1 order of magnitude lower at room temperature at $x = 0.5$ than for $BaCoO_3$. To the first approximation, there is no change in slope of the resistivity curves with Sr content, rather generally a rigid shift to lower values. The resistivity at 300 K for the most conductive compound, $Ba_{0.5}Sr_{0.5}CoO_3$, is approximately $2 \times 10^{-1}\ \Omega$-cm, still an order of magnitude larger than what might be expected for a material which is approaching metallic behavior. Plots of the temperature-dependent electrical resistivity on curves

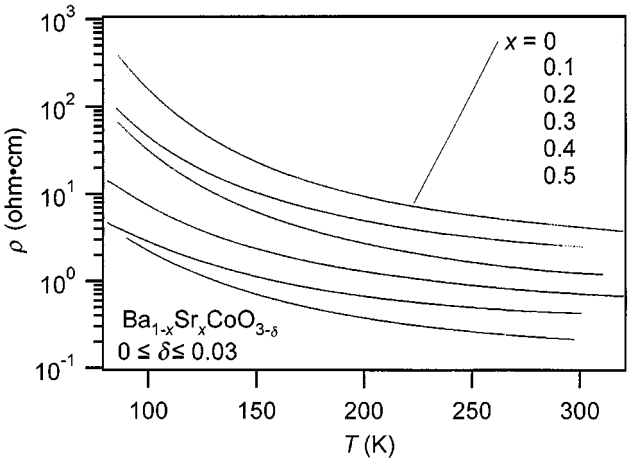

FIG. 6. The temperature dependence of electrical resistivity for polycrystalline samples of the 2H-type solid solution $Ba_{1-x}Sr_xCoO_3$ ($0 \le x \le 0.5$) as a function of Sr content.

indicative of activated resistivity ($\log \rho$ vs $1/T$), or 1D localization ($\log \rho$ vs $1/T^{1/2}$), are not straight lines. The shapes of the resistivity curves therefore do not provide sufficient evidence to determine the dominant influence on the transport properties. This may be due in part to a possible electronic anisotropy associated with the extreme structural anisotropy.

The results of measurements of the thermoelectric coefficients in the vicinity of ambient temperature for representative compositions in the solid solution are presented in Fig. 7. The thermoelectric coefficients are small and negative, indicating that the transport is dominated by n-type carriers. The thermoelectric coefficient decreases in magnitude as a function of Sr concentration. Combined with the curvature observed, and the zero crossing for the Sr concentration $x = 0.5$, the data suggest that the transport in this system is by both electrons and holes. The concentration of holelike carriers apparently increases with increasing Sr content. Alternatively, the mobilities of the holes could be increasing with increasing Sr content. The two-carrier electronic system and the highly anisotropic crystal structure suggest that single-crystal measurements parallel and perpendicular to the chain direction are needed for a more detailed understanding of the transport properties.

The Sr concentration dependence of the magnetic properties of the 2H-type solid solution was studied in a SQUID magnetometer. The temperature dependence of the magnetic susceptibility for all the final polycrystalline samples was measured under a magnetic field of 10 kOe on cooling (field cooling; FC) from 400 to 5 K. Those data are presented in Fig. 8a and 8b as χ (M/H) vs T and $1/\chi$ (H/M) vs T plots.

In the high-temperature region, above 250 K, all samples show a linear relationship between inverse magnetic susceptibility and temperature (Fig. 8b). To analyze the magnetic

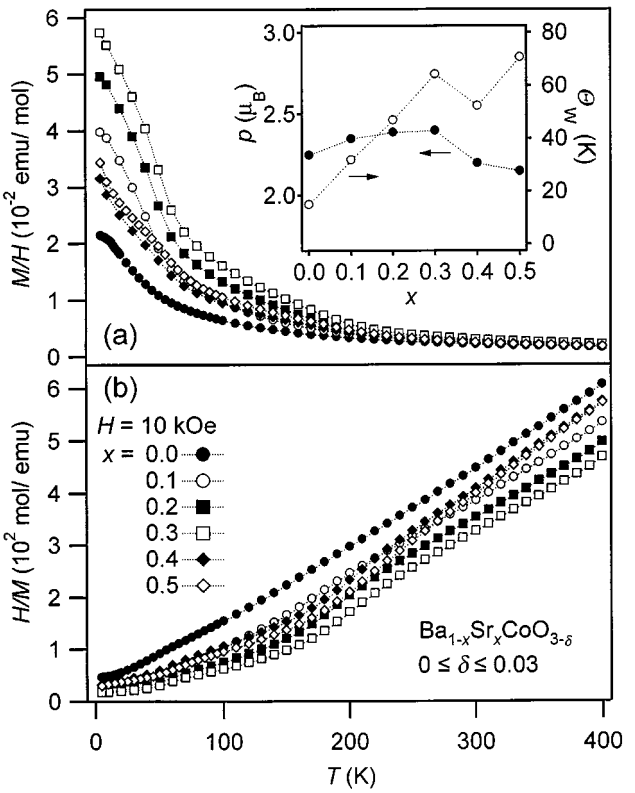

FIG. 8. (a) Temperature dependence of magnetic susceptibility (M/H) of $Ba_{1-x}Sr_xCoO_3$ ($0 \le x \le 0.5$). Each sample was cooled under an applied magnetic field of 10 kOe from 400 K. (b) Inverse plots, H/M, vs temperature. Effective magnetic moment and Weiss temperature, estimated from fits to the Curie–Weiss law above 250 K, are summarized in the insert to the upper figure.

data, several spin models were considered: a Curie–Weiss-type paramagnetic model, and 1D-Heisenberg- and Ising-type ferromagnetic chain (FM) models. For the Curie–Weiss model, the effective magnetic moment (p) and Weiss temperature (Θ_w) were estimated by least squares fitting the observed data in Fig. 8b above 250 K. The insert to Fig. 8a shows p and Θ_w as a function of Sr content. These fits clearly indicate that an electronic configuration with a low-spin state ($t_{2g}^5 e_g^0$ or its equivalent $t_{2g}^5 e_g^1 \underline{L}$; $S = 1/2$) occurs for Co, rather than one with a high-spin state, although the observed effective magnetic moment of approximately 2.3 μ_B for the whole composition range exceeds the simple estimation of 1.91 obtained by employing our preliminary room temperature electron paramagnetic resonance measurement of $g = 2.2$ and $S = 1/2$. Thus, the system can be considered as a spin 1/2 system.

To get an indication about whether the structural anisotropy is reflected in the magnetic susceptibility, the magnetic susceptibility data for $BaCoO_3$ were also fit to 1D-Heisenberg- and Ising-type FM chain models in the temperature region above 250 K. Within the Ising model, the magnetic susceptibility is expected to be $H/M = (k_B T/N) \exp(-2J/k_B T)$, $J > 0$, where k_B is the Boltzmann constant, N is Avogadro's number, T is the temperature, and J is the magnitude of the exchange interaction. The inverse magnetic susceptibility of $BaCoO_3$ is plotted in Fig. 9, with lines drawn for the expected behavior for different values of the nearest-neighbor spin interaction (J/k_B). The data indicate that within this model J/k_B can be estimated to be approximately 10 K. Above 250 K, the calculated curve is almost linear. Fit to the high-temperature expansion of the Heisenberg model also yields a J/k_B of 10 K. Hence, there is no significant difference between the fitting results for the various models in the high-temperature region where the data are free from the influence of magnetic ordering.

The Weiss temperatures are positive over the whole composition range, indicating the dominance of ferromagnetic interactions. The ferromagnetic interaction increases in strength as the Sr content is increased, as Θ_w increases from $+17$ to $+70$ K between $BaCoO_3$ and $Ba_{0.5}Sr_{0.5}CoO_3$. The significant increment in Θ_w with increasing Sr content (insert to Fig. 8a) may be due to the changing of the O–Co–O bond angle, which is expected to be an important factor in determining the magnetic superexchange, strongly influencing the inchain magnetic interactions. A detailed structural study would be required to specify the change in bond angle as a function of the Sr concentration and determine whether such a bond angle change can be the cause of the increasing ferromagnetic interaction with Sr content.

For all members of the series, the magnetic susceptibilities change character at temperatures below approximately 200 K. This is easily seen in Fig. 8b. The changes in slope suggest that at low temperatures antiferromagnetic interactions are becoming more significant. The effect is most clearly seen in the material with $x = 0.3$. For 1D spin systems, the effects of coupling between chains are expected

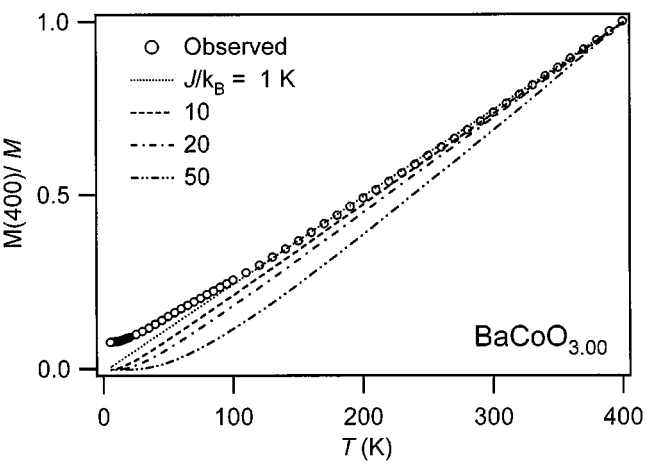

FIG. 9. Fitting results for the 1D Ising-type FM model with the parameter J, the magnitude of the nearest-neighbor spin interaction. Open circles indicate the observed temperature dependence of the inverse magnetic susceptibility of $BaCoO_3$. All are normalized at 400 K.

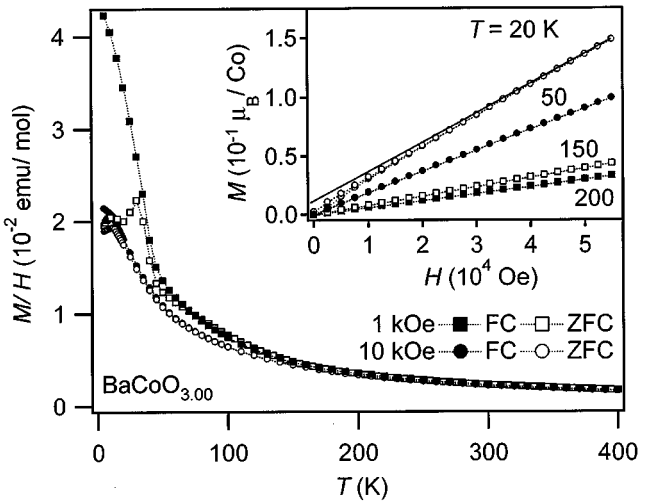

FIG. 10. Temperature dependence of the magnetic susceptibility under 1 and 10 kOe and applied magnetic field dependence of magnetization at several temperatures (insert) for $BaCoO_{3.00}$.

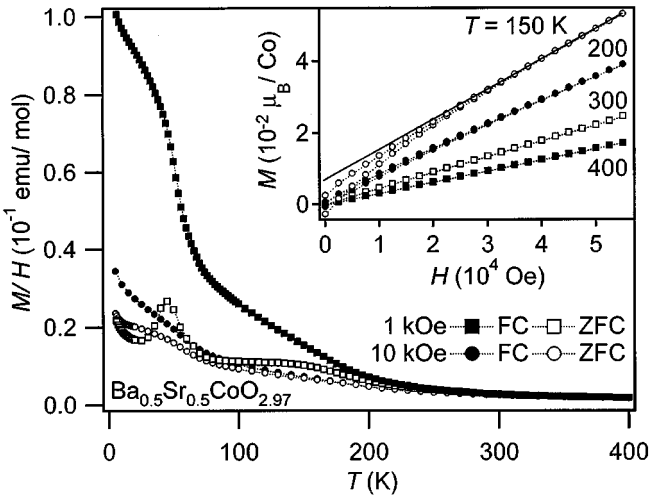

FIG. 12. Temperature dependence of the magnetic susceptibility under 1 and 10 kOe and applied magnetic field dependence of magnetization at several temperatures (insert) for $Ba_{0.5}Sr_{0.5}CoO_{2.97}$.

to appear at low temperatures (see, e.g., 14–17). The data suggest that those interchain interactions have significant antiferromagnetic character at low temperatures.

To investigate the magnetic properties further in the temperature region below 250 K, samples at $x = 0$, 0.2, and 0.5 were studied in more detail. The magnetic susceptibilities at applied fields of 1 and 10 kOe measured on heating after cooling the samples without an applied magnetic field (zero-field cooling; ZFC) and then on cooling in the field (FC) were measured. At several temperatures, the magnetic field dependence of the magnetization was measured to $\pm$ 55 kOe. The results are summarized in Figs. 10–12. In Fig. 10, for example, the summary of the data for $BaCoO_3$, the deviation between curves measured under 1 and 10 kOe below about 200 K, suggests that an ordering with a significant ferromagnetic component appears in this temperature region. The effect increases with increasing Sr content.

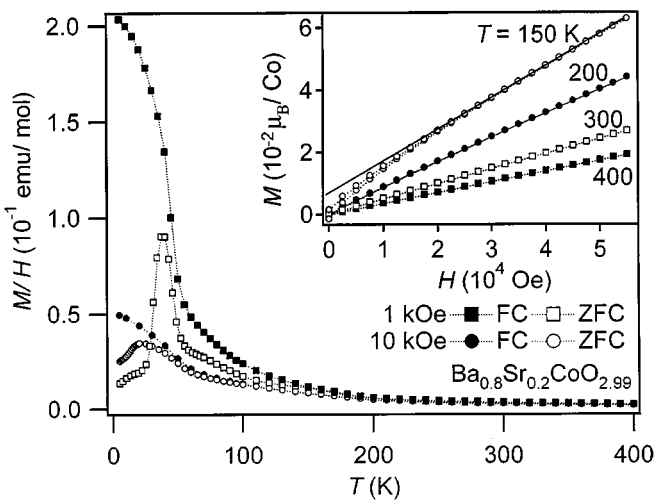

FIG. 11. Temperature dependence of the magnetic susceptibility under 1 and 10 kOe and applied magnetic field dependence of magnetization at several temperatures (insert) for $Ba_{0.8}Sr_{0.2}CoO_{2.99}$.

Below approximately 70 K, the magnetic properties of the solid solution are seen to change again. Changes in slopes of the M/H vs T curves, cusps in the M/H vs T behavior in the two ZFC curves, and increased thermal hysteresis between ZFC and FC curves measured under both magnetic field were clearly observed. The magnetic field dependence of the magnetization (insert to Figs. 10–12) reveals the presence of weak spontaneous magnetization in $BaCoO_3$ by 20 K (seen by the fact that the extrapolation of M/H to $H = 0$ is not zero). This effect also increases with increasing Sr content. A comparison of the data in Fig. 11 to those in Fig. 10, for example, indicates that the temperature of the magnetic cusps increases and that spontaneous magnetization is clearly observed at a much higher temperature (150 K) for $x = 0.2$ than for $x = 0$. By $x = 0.5$, this trend becomes even more obvious (Fig. 12).

Saturation of the magnetization was not reached under the measurement conditions. However, an order-of-magnitude estimate of the ferromagnetic contribution to the magnetization can be made from the low-temperature data (Fig. 13). For $Ba_{0.7}Sr_{0.3}CoO_3$ at 5 K, for example, in a field of 55 kOe, the magnetization is approximately on the order of 27% of the saturated moment expected for a fully ordered spin 1/2 system.

The magnetic data therefore suggest that the spin structure of the 2H-type solid solutions at low temperatures is complex. Near room temperature, Curie–Weiss-type paramagnetism is dominant. The inverse magnetic susceptibilities

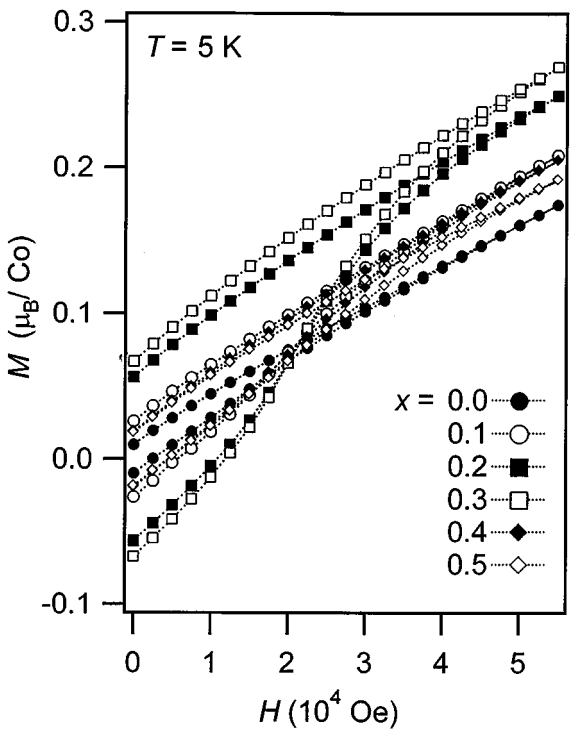

FIG. 13. Applied magnetic field dependence of the magnetization of $Ba_{1-x}Sr_xCoO_3$ ($0 \leq x \leq 0.5$) at 5 K. Saturation of the magnetization was not observed to the highest magnetic field (55 kOe).

deviate from the Curie–Weiss and 1D chain laws below approximately 200 K, consistent with the increasing influence of antiferromagnetic spin coupling. Below about 70 K, changes in slopes of the M/H vs T curves, cusps in the M/H vs T behavior in the two ZFC curves, and increased thermal hysteresis between ZFC and FC curves are observed. This appears to be due to a balance between antiferromagnetic and ferromagnetic coupling in the magnetic system. The present data are very highly reminiscent of what is seen in the one-dimensional high-spin Co-based 1D compound $Ca_3Co_2O_6$, where more extensive study has shown that the magnetic system consists of ferromagnetic chains which order ferrimagnetically at low temperatures due to antiferromagnetic coupling between chains (14–17).

CONCLUSION

The temperature-dependent magnetic susceptibility for nonsubstituted $BaCoO_3$ measured in the present study is identical to the one set of previously reported data (18). Because the maximum temperature of the measurement was 200 K in that work, a different sign for the nearest-neighbor spin interaction within the chain was proposed. The data are not in agreement with the previous report, possibly due to oxygen nonstoichiometry, as was described in (19). In the present study, the Sr-doped 2H-type compounds $Ba_{1-x}Sr_xCoO_3$ ($0 \leq x \leq 0.5$) were synthesized and studied. The structurally 1D character of the chains and their 2D packing in this crystal structure makes the magnetic and transport properties quite unusual. A more detailed study of the magnetic properties would be of interest, for instance, through neutron scattering, to fully elucidate the magnetic system, as would detailed spin-polarized band structure calculations to help clarify the relative strengths of the magnetic interactions and the temperature ranges where they may be important.

ACKNOWLEDGMENTS

We thank J. J. Krajewski for his TGA study of our preliminary samples and C. Felser and Z. Soos for helpful discussions. This work was supported in part by an Overseas Research Fellowship (K.Y.), administered by the Japan Science and Technology Corporation.

REFERENCES

1. P. W. Anderson, *Phys. Today* **50,** 42 (1997).
2. H. Taguchi, Y. Takeda, F. Kanamaru, M. Shimada, and M. Koizumi, *Acta Crystallogr. B* **33,** 1298 (1977).
3. N. Raghu, V. Ravi, and T. R. N. Kutty, *Mater. Res. Bull.* **26,** 261 (1991).
4. T. Mizokawa, H. Namatame, A. Fujimori, K. Akeyama, H. Kondoh, H. Kuroda, and N. Kosugi, *Phys. Rev. Lett.* **67,** 1638 (1991).
5. P. Kuiper, G. Kruizinga, J. Ghijisn, G. A. Sawatzky, and H. Verweij, *Phys. Rev. Lett.* **62,** 221 (1989).
6. M. A. van Veenendaal and G. A. Sawatzky, *Phys. Rev. B* **50,** 11326 (1994).
7. A. E. Bocquet, A. Fujimori, T. Mizokawa, T. Saitoh, H. Namatame, S. Suga, N. Kimizuka, Y. Takeda, and M. Takano, *Phys. Rev. B* **45,** 1561 (1992).
8. P. Bezdicka, A. Wattiaux, J. C. Grenier, M. Pouchard, and P. Hagenmuller, *Z. Anorg. Allg. Chem.* **619,** 7 (1993).
9. N. Nakamura, A. Sekiyama, H. Namatame, A. Fujimori, H. Yoshihara, T. Ohtani, A. Misu, and M. Takano, *Phys. Rev. B* **49,** 16191 (1994).
10. A. Varela, M. Parras, K. Boulahya, and J. M. Gonzalez-Calbet, *J. Solid State Chem.* **128,** 130 (1997).
11. M. Parras, A. Varela, H. Seehofer, and J. M. Gonzalez-Calbet, *J. Solid State Chem.* **120,** 327 (1995).
12. A. J. Jacobson and J. L. Hutchison, *J. Solid State Chem.* **35,** 334 (1980).
13. R. D. Shannon, *Acta Crystallogr. Sect. A* **32,** 751 (1976).
14. H. Fjellvag, E. Gulbrandsen, S. Aasland, A. Olsen, and B. C. Hauback, *J. Solid State Chem.* **124,** 190 (1996).
15. H. Kageyama, K. Yoshimura, K. Kosuge, H. Mitamura, and T. Goto, *J. Phys. Soc. Jpn.* **66,** 1607 (1997).
16. H. Kageyama, K. Yoshimura, K. Kosuge, X. Xu, and S. Kawano, *J. Phys. Soc. Jpn.* **67,** 357 (1998).
17. H. Kageyama, K. Yoshimura, K. Kosuge, H. Nojiri, K. Owari, and M. Motokawa, *Phys. Rev. B* **58,** 11150 (1998).
18. Y. Takeda, *J. Solid State Chem.* **15,** 40 (1975).
19. G. A. Candela, A. H. Kahn, and T. Negas, *J. Solid State Chem.* **7,** 360 (1973).